ISSN 0023-1584, Kinetics and Catalysis, 2008, Vol. 49, No. 5, pp. 676–681. © Pleiades Publishing, Ltd., 2008.
Published in Russian in Kinetika i Kataliz, 2008, Vol. 49, No. 5, pp. 707–712.

Preparation of Mesoporous $Ce_{1-x}Fe_xO_2$ Mixed Oxides and Their Catalytic Properties in Methane Combustion[1]

Chengwen Liu, Laitao Luo, and Xun Lu

Department of Chemistry, NanChang University, NanChang, 330031, P.R. China

e-mail: luolaitao@163.com

Received July 7, 2007

Abstract—Mesoporous $Ce_{1-x}Fe_xO_2$ mixed oxide catalysts of different molar ratios (x = 0.1–0.5) were prepared by the citric acid sol-gel method and the microwave technique. The activities of $Ce_{1-x}Fe_xO_2$ mixed oxides on methane combustion were investigated, and the structure and reductive properties were characterized by XRD, BET, DRS, and TPR. The data showed that $Ce_{1-x}Fe_xO_2$ mixed oxides prepared were mesoporous material. When $x \le 0.2$, the transition metal Fe incorporated into the lattice of CeO_2 to form cubic $Ce_{1-x}Fe_xO_2$ solid solutions, and mixed phases of cubic $Ce_{1-x}Fe_xO_2$ solid solutions and α-Fe_2O_3 existed when $x > 0.2$. $Ce_{1-x}Fe_xO_2$ solid solutions show higher activity for methane combustion than pure CeO_2, especially for $Ce_{0.9}Fe_{0.1}O_2$.

DOI: 10.1134/S0023158408050121

1. INTRODUCTION

Catalytic combustion has attracted much attention due to the high combustion efficiency as well as the low emission of air pollutants such as CO, NO_x, and unburned hydrocarbons [1–6]. For a long time, supported noble metal catalysts have generally been used for methane combustion [7, 8]. However, supported noble metal catalysts, although with outstanding activity, are not fully satisfactory based on the high price and scarce resources. Therefore, there is a strong demand for the development of new, thermally stable and low-cost catalysts for the combustion of methane. Recently, various transition metal oxide catalysts have been investigated as a substitute for the noble metal catalysts in methane combustion [9–11]. Several types of catalysts have been developed at various stages; particular attention is being paid to ceria-based catalysts, and specifically CeO_2-containing mixed oxides having a fluorite structure. Ceria has been widely used as a promoter and an oxidation catalyst because of its unique redox properties and high oxygen storage capacity [12, 13]. Nowadays, the rapid growth in applications and characterization of CeO_2-containing catalysts have been well documented [14, 15]. The important role of ceria is reported to be the generation and participation of surface oxygen species and anionic vacancies in the catalytic reactions [16]. Many studies have indicated that these redox properties can be enhanced considerably if additional elements are introduced into the CeO_2 lattice by forming solid solutions [17].

The pore sizes of mesoporous materials are usually 2–50 nm; they have high surface area and moderate pore structure, which are advantageous to the adsorption, diffusion, and reaction of organic molecules on surfaces of catalyst. In our recent works, mesoporous $Ce_{1-x}Fe_xO_2$ mixed oxide catalysts were prepared by the sol-gel method and microwave technique, and their textures, reduction properties, and catalytic activities for methane combustion were investigated.

2. EXPERIMENTAL

2.1. Preparation of the Catalyst

$Ce_{1-x}Fe_xO_2$ (x = 0.1–0.5) mixed oxide catalysts were prepared by the citric acid sol-gel method. An appreciate amount of citric acid solid powder was added to the mixed nitrate solution of cerium and iron. The mixed solution was then vaporized at 80°C under stirring, dried by microwave, and calcined at 700°C for 4 h in air. Single CeO_2 and Fe_2O_3 catalysts were obtained by the same method.

2.2. BET Surface Area

The BET surface area and porous texture were evaluated by N_2 adsorption isotherms obtained at 77 K in an ASAP 2020 (Micrometrics) equipment. Before each measurement, the catalysts were degassed in vacuum at 623 K for 1 h. The calculation of pore size and pore volume were based on the BJH equation.

2.3. X-Ray Powder Diffraction (XRD)

The phase composition of the various samples was determined by XRD, using a Rigaku D/max-3BX. The operating parameters were monochromatic CuK_α radi-

[1] The text was submitted by the authors in English.

ation, Ni filter, 40 mA, and 40 kV, 2θ scanning from 20° to 80°.

2.4. Temperature-Programmed Reduction (TPR)

The temperature-programmed reduction spectra were obtained on a homemade apparatus loaded with 0.1 g catalyst. The catalyst was pretreated in N_2 at 700°C for 2 h prior to measurement. The reduction gas is a gas mixture of 10 vol % H_2/N_2. The temperature of the sample is programmed to rise at 800°C with a constant rate of 10 K/min. H_2 consumption during the reduction was measured by a TCD.

2.5. UV Diffuse Reflectance Spectra (DRS)

DRS of the samples were recorded in the 200–800 nm range with a Cary 500 spectrophotometer, using $BaSO_4$ as a reference.

2.6. Catalytic Activity Tests

The reaction of methane combustion is carried out in a conventional flow system under atmospheric pressure. For each experiment, 0.1 g of catalyst (60–80 mesh) was used; the space velocity was 15000 h^{-1}; and the composition of the mixture gases was CH_4, 4 vol %, O_2, 12.5 vol %, and N_2, 83.5 vol %. The effluent gas was analyzed by on-line gas chromatography.

3. RESULTS AND DISCUSSION

3.1. Specific Surface Area and Pore Size Distribution

The nitrogen adsorption–desorption isotherms and pore size distributions performed on the desorption branch of mesoporous $Ce_{1-x}Fe_xO_2$ mixed oxide samples calcined at 700°C are shown in Fig. 1, which exhibits a typical IV type as defined by IUPAC [18]. The P/P_0 position of the inflection points is related to the diameter in the mesopore range, and the pore size distribution plots indicate that the amount of doped Fe in ceria has a great effect on the porosity of $Ce_{1-x}Fe_xO_2$ mixed oxides. The pore size distribution of $Ce_{0.9}Fe_{0.1}O_2$ is narrow and centered at 6.3 nm indicating the texture uniformity of this sample. An increase in the pore size and a broader size distribution are observed at an increasing iron content for $Ce_{1-x}Fe_xO_2$ mixed oxide catalysts. In addition, the specific surface area of $Ce_{1-x}Fe_xO_2$ mixed oxides decreased from 38.4 to 5.1 m^2/g with an increase in the Fe content, which indicates that the $Ce_{1-x}Fe_xO_2$ mixed oxide has a higher specific surface area and narrow pore size distribution when a small amount of Fe was doped.

3.2. XRD Patterns

The X-ray diffraction patterns of CeO_2 and $Ce_{1-x}Fe_xO_2$ mixed oxide samples are shown in Fig. 2. The XRD peaks for pure ceria are observed at 2θ = 28.8°, 33.4°, 47.7°, and 56.7° corresponding to the (1 1 1), (2 0 0), (2 2 0), and (3 1 1) planes, respectively. The diffraction peaks are characteristic of the cubic ceria phase with fluorite structure (JCPDS card number 34-394). No diffraction peaks of α-Fe_2O_3 in $Ce_{1-x}Fe_xO_2$ catalysts are observed when $x < 0.2$, indicating that α-Fe_2O_3 are highly dispersed in the catalyst surface or pure (Fig. 2). It can be seen that the lattice parameters of ceria decrease with the addition of Fe^{3+}, suggesting that some Fe^{3+} ions are incorporated into ceria lattice to form solid solution of $Ce_{1-x}Fe_xO_2$, as the radius of Fe ion (0.060 nm) is smaller than that of Ce^{4+} ion (0.087 nm). Diffraction peaks of α-Fe_2O_3 in $Ce_{1-x}Fe_xO_2$ catalysts are observed at 2θ = 24.1°, 35.6°, 49.5°, and 54.1° when $x > 0.2$, and the intensity of the α-Fe_2O_3 diffraction peaks increases with increasing content of Fe^{3+}.

Catalysts composition, surface area (S_{BET}), lattice constant (a), and average crystal grain size (D)

Samples	S_{BET}, m^2/g	a, nm	D, nm
CeO_2	29.4	0.5427	24.28
$Ce_{0.9}Fe_{0.1}O_2$	38.4	0.5422	15.54
$Ce_{0.8}Fe_{0.2}O_2$	35.4	0.5417	15.50
$Ce_{0.7}Fe_{0.3}O_2 + Fe_2O_3$	5.1	0.5413	35.18
$Ce_{0.6}Fe_{0.4}O_2 + Fe_2O_3$	9.1	0.5410	37.18
$Ce_{0.5}Fe_{0.5}O_2 + Fe_2O_3$	7.4	0.5407	41.72
Fe_2O_3	3.2		

The average crystal grain size (D) of iron-substituted ceria powders, calculated by the Scherrer formula from the XRD data, are listed in the table. As for $x \le 0.2$, D are smaller than those of other catalysts; when $x > 0.2$, D are larger, which may be caused by some α-Fe_2O_3 aggregate in the surface of the catalysts.

3.3. UV-vis Diffuse Reflectance

The UV spectra of $Ce_{1-x}Fe_xO_2$ mixed oxides, pure CeO_2 and Fe_2O_3 are presented in Fig. 3. The UV spectra of NaO_2 prepared by the sol-gel method show two intense bands at 256 and 296 nm in Fig. 3, curve *1*. The distinct absorption bands are assigned to the $O_2 \longrightarrow Ce^{3+}$ and $O^{2-} \longrightarrow Ce^{4+}$ charge transfer transitions [19]. Pure Fe_2O_3 shows a broad absorption feature around 560 nm in Fig. 3, curve *7*. This absorption feature is a characteristic of the *d–d* transitions of octahedrally coordinated Fe^{3+} ions [20].

Adding a small amount Fe^{3+} ($x \le 0.2$) to ceria does not change the absorption features of the UV spectra of ceria, which is likely attributed to the fact that Fe^{3+} has been incorporated into the lattice of ceria forming $Ce_{1-x}Fe_xO_2$ solid solutions. The absorption band at 560 nm of α-Fe_2O_3 is observed when Fe^{3+} ($x > 0.2$) in

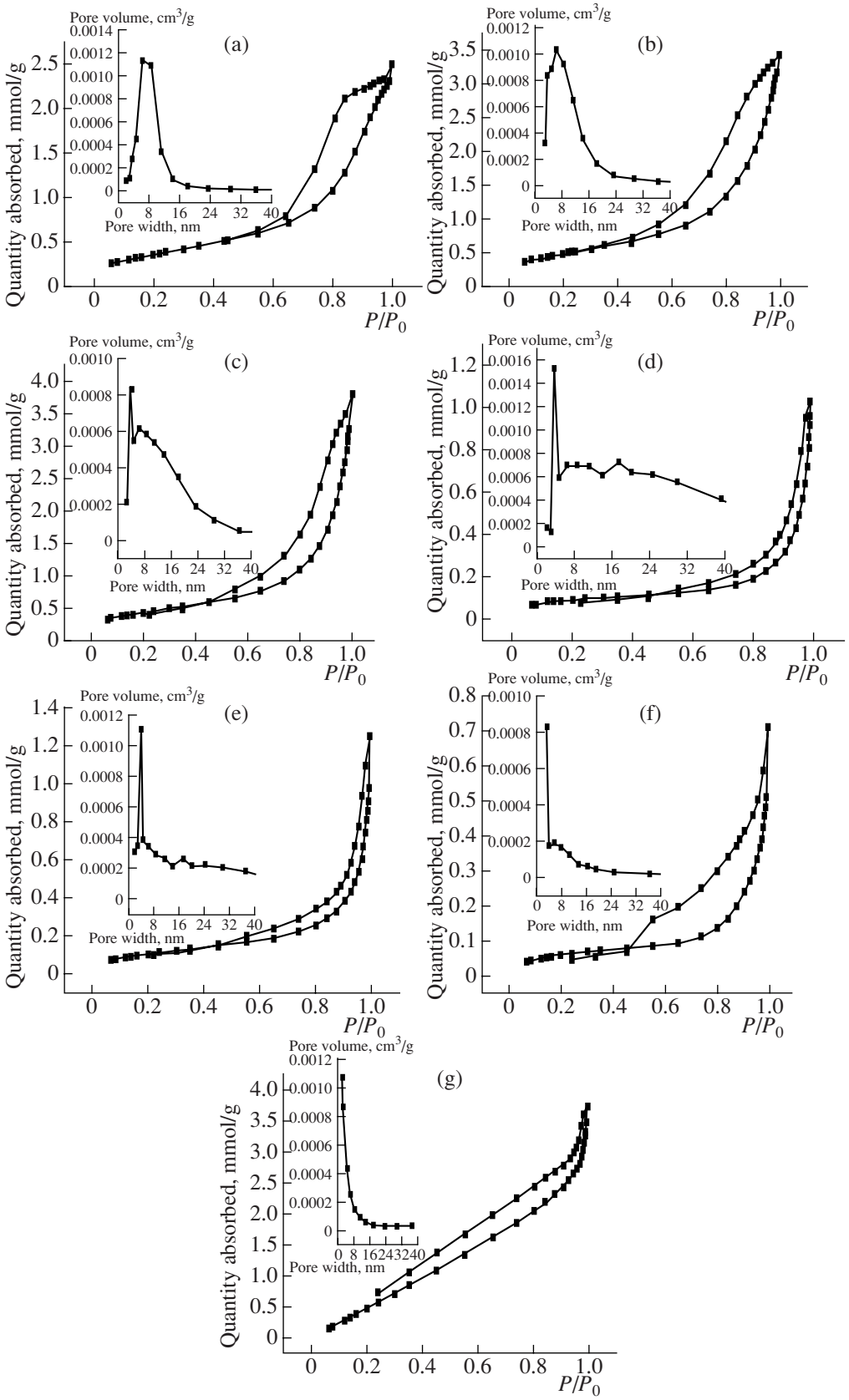

Fig. 1. N_2 adsorption–desorption isotherms and BJH pore size distribution (inset) of $Ce_{1-x}Fe_xO_2$ mixed oxide catalysts.

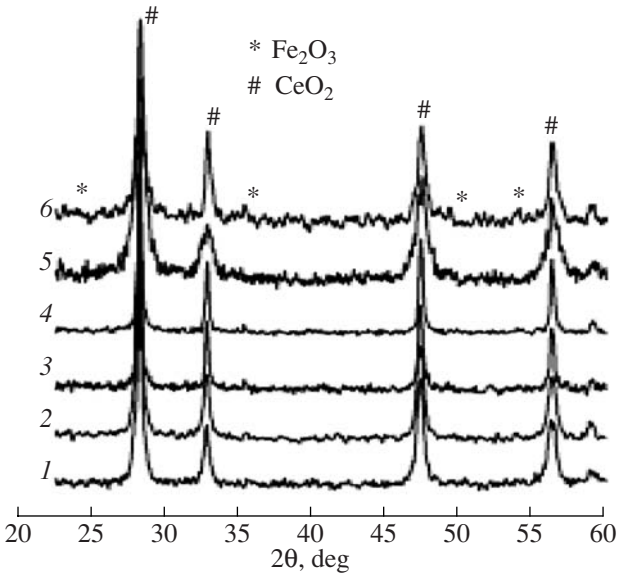

Fig. 2. XRD patterns of $Ce_{1-x}Fe_xO_2$. (*1*) CeO_2; (*2*) $Ce_{0.9}Fe_{0.1}O_2$; (*3*) $Ce_{0.8}Fe_{0.2}O_2$; (*4*) $Ce_{0.7}Fe_{0.3}O_2$; (*5*) $Ce_{0.6}Fe_{0.4}O_2$; (*6*) $Ce_{0.5}Fe_{0.5}O_2$.

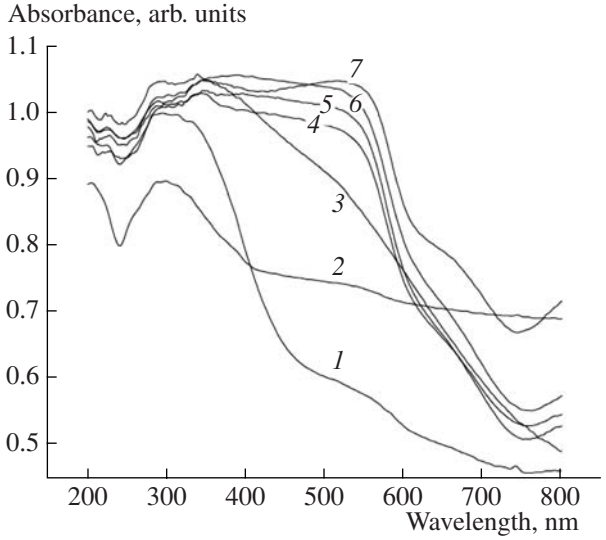

Fig. 3. The UV–vis DRS spectra of $Ce_{1-x}Fe_xO_2$ catalysts (*1*) CeO_2; (*2*) $Ce_{0.9}Fe_{0.1}O_2$; (*3*) $Ce_{0.8}Fe_{0.2}O_2$; (*4*) $Ce_{0.7}Fe_{0.3}O_2$; (*5*) $Ce_{0.6}Fe_{0.4}O_2$; (*6*) $Ce_{0.5}Fe_{0.5}O_2$; (*7*) Fe_2O_3.

$Ce_{1-x}Fe_xO_2$, indicating that some Fe^{3+} cannot be incorporated into the CeO_2 lattice; the result is consistent with the results of XRD.

3.4. Reduction Properties of the Catalysts

The H_2-TPR profiles of CeO_2, Fe_2O_3, and $Ce_{1-x}Fe_xO_2$ mixed oxides are shown in Fig. 4. The reduction peak of pure CeO_2 observed at the temperature of 635°C is attributed to the reduction of surface CeO_2. The Fe_2O_3 TPR profile presents two peaks, suggesting a two-step process. The first temperature signal, at 439°C, is attributed to the reduction of α-Fe_2O_3 to Fe_3O_4, whereas the second one, at 674°C, can be ascribed to the reduction of Fe_3O_4 to Fe, which would proceed through the following reaction steps [21]: $H_2 + 3\alpha\text{-}Fe_2O_3 \longrightarrow 2Fe_3O_4 + H_2O$ and $Fe_3O_4 + 4H_2 \longrightarrow 3Fe + 4H_2O$. By contrast, the TPR profiles of the $Ce_{1-x}Fe_xO_2$ mixed oxides show a new peak at temperatures lower than 320°C, which can be ascribed to the reduction of adsorbed oxygen species. It was generally accepted that the formation of solid solution of $Ce_{1-x}Fe_xO_2$ by the incorporation of Fe^{3+} ions into the ceria lattice would result in the generation of oxygen vacancies, leading to adsorbed oxygen in oxygen vacancies reducible by H_2 at low temperature. It also can be seen that the reduction temperature of ceria in $Ce_{0.9}Fe_{0.1}O_2$ mixed oxides shifts to a lower temperature, which indicates a higher mobility of the lattice oxygen, while for $Ce_{1-x}Fe_xO_2$ ($x \geq 0.2$), the peak position is almost unaffected by increasing the amount of Fe_2O_3 from 20 to 50%. An increase in the intensity of the peak areas is observed, which means that there are more Ce^{4+} reduced to Ce^{3+}, and all of these benefit the combustion of methane. The peak at 749°C for $Ce_{1-x}Fe_xO_2$ ($x \geq 0.3$) can be ascribed to the reduction of Fe_2O_3. The reduction shift to the higher temperature of Fe_2O_3 can be ascribed to the strong interactions between Fe and Ce.

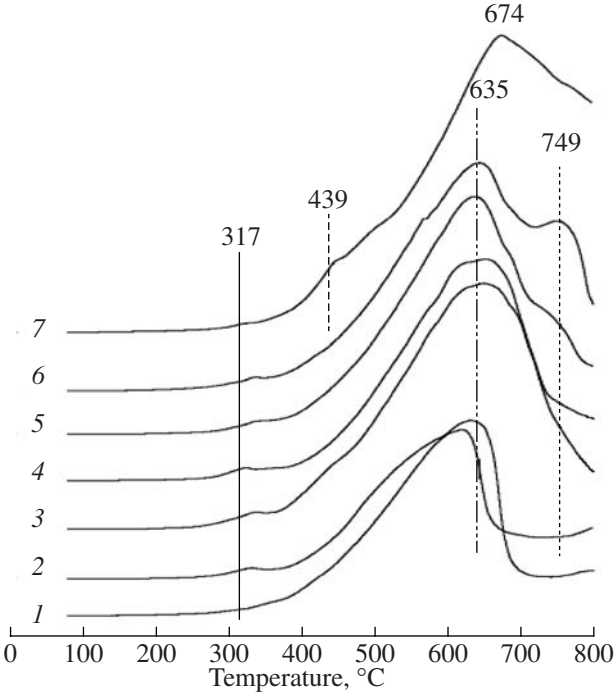

Fig. 4. TPR profiles of $Ce_{1-x}Fe_xO_2$. (*1*) CeO_2; (*2*) $Ce_{0.9}Fe_{0.1}O_2$; (*3*) $Ce_{0.8}Fe_{0.2}O_2$; (*4*) $Ce_{0.7}Fe_{0.3}O_2$; (*5*) $Ce_{0.6}Fe_{0.4}O_2$; (*6*) $Ce_{0.5}Fe_{0.5}O_2$; (*7*) Fe_2O_3.

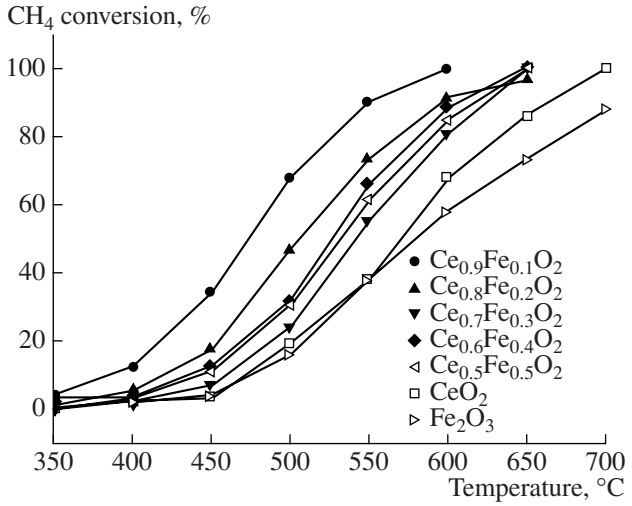

Fig. 5. Catalytic activity of $Ce_{1-x}Fe_xO_2$ in methane combustion.

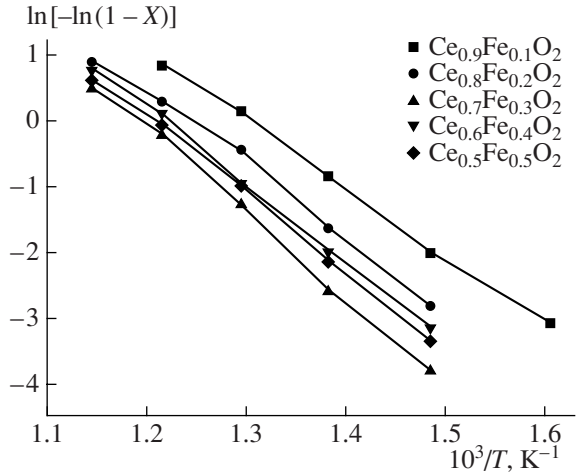

Fig. 6. Arrhenius plots for Ce–Fe–O mixed oxide catalysts.

3.5. Catalytic Activity

The catalytic behavior of the $Ce_{1-x}Fe_xO_2$ mixed oxide catalysts prepared by the sol-gel method have been tested in the methane combustion reaction. In all cases, carbon monoxide is not formed and the carbon dioxide selectivity is almost 100%. Figure 5 showed the catalytic combustion performance of the $Ce_{1-x}Fe_xO_2$ mixed oxide catalysts. Obviously, the activity of $Ce_{1-x}Fe_xO_2$ mixed oxides is better than that of single Fe_2O_3 or CeO_2. The temperatures for T_{10} (10% conversion of methane) and T_{90} (90% conversion of methane) for methane combustion over $Ce_{0.9}Fe_{0.1}O_2$ are 388°C and 550°C, respectively, which are 86 and 113°C lower than the corresponding temperatures of T_{10} or T_{90} over CeO_2. Although $Ce_{0.9}Fe_{0.1}O_2$ is still a Ce-rich catalyst, its conversion temperature of methane is far lower than CeO_2, indicating that the presence of a small amount of Fe^{3+} can significantly enhance its activity. In conclusion, it seems that what makes doped ceria more active is the increase of oxygen mobility or more reducible species, which is the result of introduction of defect sites. In general, it is commonly accepted that the catalytic activity in light alkane combustion is proportional to the surface area and the amount of the incorporated active components [22]. It can be seen that the BET specific surface area of $Ce_{0.9}Fe_{0.1}O_2$ and $Ce_{0.8}Fe_{0.2}O_2$ is significantly higher than those of others. Thus, it is likely that the increased methane combustion activity is strongly related to the much higher surface area of $Ce_{0.9}Fe_{0.1}O_2$. One can also see that $Ce_{0.9}Fe_{0.1}O_2$ has a narrow pore size distribution, which may be beneficial to methane combustion.

It is reported that the methane combustion process is according to a redox mechanism, for which several kinetic models for the reaction rate have been proposed [23–27]. The rate is considered to be first-order in the CH_4 partial pressure, whereas the order with respect to oxygen might be variable from 0 to 0.5. For a simple first-order kinetic model, the reaction rate is

$$r_{CH_4} = kP_{CH_4},$$

where k is the specific rate constant and P_{CH_4} is the methane partial pressure. By combining the design equation for the plug-flow reactor and the Arrhenius equation, the following relationship can be established [28]:

$$\ln[-\ln(1-X)] = \ln A - E_a/RT,$$

where x is the CH_4 conversion, A is the preexponential factor, T is the reaction temperature in K, E_a is the apparent activation energy, and R is the gas constant. A plot of $\ln[-\ln(1-x)]$ versus $1/T$ is shown in Fig. 6. The results fit the simple first-order model well. Apparent activation energies of 85.94, 95.75, 109.92, 97.25, and 98.87 kJ/mol were calculated for the $Ce_{0.9}Fe_{0.1}O_2$, $Ce_{0.8}Fe_{0.2}O_2$, $Ce_{0.7}Fe_{0.3}O_2$, $Ce_{0.6}Fe_{0.4}O_2$, and $Ce_{0.5}Fe_{0.5}O_2$, respectively. The slightly lower activation energy measured for $Ce_{0.9}Fe_{0.1}O_2$ indicates the higher activity of this system.

4. CONCLUSIONS

Mesoporous $Ce_{1-x}Fe_xO_2$ mixed oxide catalysts were prepared by the citric sol-gel method and microwave technique. The catalysts exhibit remarkably high catalytic activity in the catalytic methane combustion, especially for $Ce_{0.9}Fe_{0.1}O_2$. Combined BET, XRD, DRS, and TPR results demonstrated that the superior catalytic performance of the $Ce_{1-x}Fe_xO_2$ mixed oxide catalysts could be attributed to the generation of oxygen vacancies, more reducible species, high surface area, and moderate pore sizes by the formation of solid solutions.

ACKNOWLEDGMENTS

This work was supported by the fund of Doctoral Degree Special Scientific Research of the Ministry of Education of P.R. China (Project 20040403001).

REFERENCES

1. Trimm, D.L., *Appl. Catal.*, 1983, vol. 7, p. 249.
2. Prasad, R., Kennedy, L.A., and Ruckentein, E., *Catal. Rev.*, 1984, vol. 26, p. 1.
3. Forzatti, P. and Groppi, G., *Catal. Today*, 1999, vol. 54, p. 165.
4. Wierzba, I. and Depiak, A., *Int. J. Hydrogen Energy*, 2004, vol. 29, p. 1303.
5. Choudhary, T.V., Banerjee, S., and Choudhary, V.R., *Appl. Catal., A*, 2002, vol. 234, p. 1.
6. Corro, G., Fierro, J.L.G., and Vázquez, O.C., *Catal. Commun.*, 2005, vol. 6, p. 287.
7. Widjaja, H., Sekizawa, K., Eguchi, K., and Arai, H., *Catal. Today*, 1999, vol. 47, p. 95.
8. Baiker, A., Marti, P.E., Keusch, P., Fritsch, E., and Reller, A., *J. Catal.*, 1994, vol. 146, p. 268.
9. Saracco, G., Scibilia, G., Iannibello, A., and Baldi, G., *Appl. Catal., B*, 1996, vol. 8, p. 229.
10. Artizzu, P., Garbowski, E., Primet, M., Brulle, Y., and Saint-Just, J., *Catal. Today*, 1999, vol. 47, p. 83.
11. Rosso, I., Saracco, G., Specchia, V., and Garrone, E., *Appl. Catal., B*, 2003, vol. 40, p. 195.
12. Otsuka, K., Ye, W., and Nakamura, M., *Appl. Catal., A*, 1999, vol. 183, p. 317.
13. Trovarelli, A., de Leitenburg, C., Boaro, M., and Dolcetti, G., *Catal. Today*, 1999, vol. 50, p. 353.
14. Trovarelli, A., *Catal. Rev.*, 1996, vol. 38, p. 439.
15. Wang, J.B., Shih, W.H., and Huang, T.J., *Appl. Catal., A*, 2000, vol. 203, p. 191.
16. Trovarelli, A., De Leitenburg, C., Llorca, J., and Dolcetti, G., *J. Catal.*, 1995, vol. 151, p. 111.
17. Wrobel, G., Lamonier, C., Bennani, A., Huysser, A., and Aboukas, A., *J. Chem. Soc., Faraday Trans.*, 1996, vol. 92, p. 2001.
18. Sing, K.S.W., Everett, D.H., Haul, R.A., Moscow, L., Pierotti, R.A., Rouquerol, J., and Siemieniewska, T., *Pure Appl. Chem.*, 1985, vol. 57, p. 603.
19. Bensalem, A., Muller, J.C., and Bozon-Verduraz, F., *J.Chem.Soc. Faraday Trans*, 1992, vol. 88, p. 153.
20. Groppi, G., Cristiani, C., and Forzatti, P., *J. Catal.*, 1997, vol. 168, p. 95.
21. Unmuth, E.E., Schwartz, L.H., and Butt, J.B., *J. Catal.*, 1980, vol. 61, p. 242.
22. Cho, S.J., Song, K.S., Ryu, I.S., Seo, Y.S., Ryoo, M.W., and Kang, S.K., *Catal. Lett.*, 1999, vol. 58, p. 63.
23. Tejuca, L.G., Fierro, J.L.G., and Fascon, J.M.D., *Adv. Catal.*, 1989, p. 327.
24. Pena, M.A. and Fierro, J.L.G., *Chem. Rev.*, 2001, vol. 101, p. 1981.
25. Aria, H., Yamada, T., and Seiyama, T., *Appl. Catal.*, 1986, vol. 26, p. 265.
26. Ladavos, A.K. and Pimonis, P.J., *J. Chem. Soc., Faraday Trans.*, 1992, vol. 88, p. 25.
27. Saracco, G., Geobaldo, F., and Baldi, G., *Appl. Catal., B*, 1999, vol. 20, p. 277.
28. Falcon, H., Barbero, J.A., Alonso, J.A., Martinez-Lope, M.J., and Fierro, J.L.G., *Chem. Mater.*, 2002, vol. 142, p. 325.